NANO · MICRO small
www.small-journal.com

Engineering pH-Sensitive Stable Nanovesicles for Delivery of MicroRNA Therapeutics

Ariadna Boloix, Natalia Feiner-Gracia, Mariana Köber, Javier Repetto, Rosa Pascarella, Aroa Soriano, Marc Masanas, Nathaly Segovia, Guillem Vargas-Nadal, Josep Merlo-Mas, Dganit Danino, Inbal Abutbul-Ionita, Laia Foradada, Josep Roma, Alba Córdoba, Santi Sala, Josep Sánchez de Toledo, Soledad Gallego, Jaume Veciana, Lorenzo Albertazzi, Miguel F. Segura, and Nora Ventosa**

MicroRNAs (miRNAs) are small non-coding endogenous RNAs, which are attracting a growing interest as therapeutic molecules due to their central role in major diseases. However, the transformation of these biomolecules into drugs is limited due to their unstability in the bloodstream, caused by nucleases abundantly present in the blood, and poor capacity to enter cells. The conjugation of miRNAs to nanoparticles (NPs) could be an effective strategy for their clinical delivery. Herein, the engineering of non-liposomal lipid nanovesicles, named quatsomes (QS), for the delivery of miRNAs and other small RNAs into the cytosol of tumor cells, triggering a tumor-suppressive response is reported. The engineered pH-sensitive nanovesicles have controlled structure (unilamellar), size (<150 nm) and composition. These nanovesicles are colloidal stable (>24 weeks), and are prepared by a green, GMP compliant, and scalable one-step procedure, which are all unavoidable requirements for the arrival to the clinical practice of NP based miRNA therapeutics. Furthermore, QS protect miRNAs from RNAses and when injected intravenously, deliver them into liver, lung, and neuroblastoma xenografts tumors. These stable nanovesicles with tunable pH sensitiveness constitute an attractive platform for the efficient delivery of miRNAs and other small RNAs with therapeutic activity and their exploitation in the clinics.

1. Introduction

RNA-based therapeutics have the potential to target all the transcriptome, expanding the number of druggable targets.[1] MicroRNA (miRNA) are endogenous non-coding small RNA (sRNA) that interfere with the translation and stability of coding and non-coding messenger RNA (mRNA) in a sequence-specific manner.[2] miRNA are promising therapeutic tools owing to their ability of regulate multiple genes and/or pathways simultaneously.[3] However, in vivo administration of naked RNA faces limitations, such as, low cellular uptake, degradation by nucleases, and rapid clearance, among others.[4,5] Therefore, nanocarriers such as positively charged nanoparticles (NPs) are investigated for RNA delivery[6] due to their capacity to complex these negatively charged biomolecules through electrostatic interactions and to transport them to the desired site of action.[3] Positively charged NPs developed thus far—mostly liposomes, polymeric,

A. Boloix, M. Köber, J. Repetto, N. Segovia, G. Vargas-Nadal, J. Veciana, N. Ventosa
Molecular Nanoscience and Organic Materials (Nanomol)
Institut de Ciència de Materials de Barcelona
ICMAB-CSIC
Campus UAB
Bellaterra 08193, Spain
E-mail: ventosa@icmab.es

The ORCID identification number(s) for the author(s) of this article can be found under https://doi.org/10.1002/smll.202101959.

DOI: 10.1002/smll.202101959

A. Boloix, A. Soriano, M. Masanas, J. Roma, J. S. Toledo, S. Gallego, M. F. Segura
Laboratory of Translational Research in Childhood and Adolescent Cancer
Vall d'Hebron Research Institute (VHIR)-UAB
Barcelona 08035, Spain
E-mail: miguel.segura@vhir.org

A. Boloix, M. Köber, N. Segovia, G. Vargas-Nadal, J. Veciana, N. Ventosa
CIBER de Bioingeniería
Biomateriales y Nanomedicina (CIBER-BBN)
Madrid 28029, Spain

N. Feiner-Gracia, R. Pascarella, L. Albertazzi
Nanoscopy for Nanomedicine Group
Institute for Bioengineering of Catalonia (IBEC)
The Barcelona Institute of Science and Technology (BIST)
Barcelona 08024, Spain

and other lipid NPs[7–9]—have failed at clinical stages mainly due to low colloidal stability upon storage,[10,11] high polydispersity,[11] and difficulties to scale-up the NPs production[12] or unexpected toxicities at repeated doses.[11,13,14]

Despite multiple pharmaceutical companies have already included miRNA in their developmental drug pipelines (e.g., miR-34,[15] miR-16,[16] miR-122[17]), none of these miRNA have as yet been introduced into clinical practice for cancer treatment.

Here, we report stable nanovesicles, based on quatsomes (QS), with tunable pH sensitiveness for systemic delivery of miRNA. QS are unilamellar non-liposomal lipid-based nanovesicles, formed by the self-assembly of sterols and quaternary ammonium surfactants, characterized with a permanent positive charge and long-term stability upon storage.[10,18]

The pH-sensitive QS presented here contain the sterol derivative cholesteryl *N*-(2-dimethylaminoethyl)carbamate (DC-Chol), a weak base with a tertiary amine that is protonated/deprotonated in a pH-dependent manner, facilitating the complexation/decomplexation of the negatively-charged miRNA as a function of pH. The behavior of QS in response to pH can be designed "on-demand" by changing the DC-Chol content in their membrane.

QS are prepared by a one-step, GMP compliant scalable technology,[19] named DELOS-SUSP, which uses green compressed CO_2 and allows the production of nanovesicular formulations with a high nanovesicle-to-nanovesicle homogeneity, appropriate for in vivo administration.[20,21] Importantly, the surface of our QS can easily be functionalized with stealth groups (like PEGs),[20] targeting units,[20] and/or fluorophores, to target specific tissues and/or perform bio-imaging.[22–24]

To demonstrate the functionality of pH sensitive QS for miRNA delivery, we selected neuroblastoma, an aggressive pediatric tumor that demands new therapies. Neuroblastomas are the most common extracranial solid tumor in children, representing ≈8–10% of childhood cancers, and causing ≈15% of all pediatric cancer deaths.[25] Particularly, high-risk neuroblastoma patients face poor outcomes since the approved therapies for refractory or relapsed tumors are scant.[26] We and others have described multiple miRNAs with tumor-suppressive functions,[27] including miR-323a-5p, the restoration of which reduced neuroblastoma growth in vitro and in vivo by targeting cell proliferation and survival related genes.[28] In the present work, we show the efficiency of QS nanovesicles to deliver miR-323a-5p to neuroblastoma, eliciting an antitumoral response. Furthermore, QS-miRNA complexes protect miRNAs from nuclease degradation and, when injected intravenously, are capable of raising miRNA levels in tissues such as liver, lung, or xenografted neuroblastoma tumors, among others. The efficiency of these stable nanovesicles is also demonstrated with other small RNAs, such as, small interfering RNA (siRNA). The results presented here justify further exploration of this new type of nanocarrier for clinical administration of sRNAs to treat cancer such as, high-risk neuroblastoma and other diseases related to miRNA disfunction.

N. Feiner-Gracia, R. Pascarella, L. Albertazzi
Department of Biomedical Engineering
Institute for Complex Molecular Systems (ICMS)
Eindhoven University of Technology
Eindhoven 5612AZ, The Netherlands

J. Merlo-Mas, A. Córdoba, S. Sala
Nanomol Technologies SL
Campus de la UAB
Bellaterra 08193, Spain

D. Danino, I. Abutbul-Ionita
CryoEM Laboratory of Soft Matter
Technion - Israel Institute of Technology
Haifa 32000, Israel

D. Danino
Guangdong Technion - Israel Institute of Technology
Shantou, Guangdong Province 515063, China

L. Foradada
Peptomyc S.L.
Vall d'Hebron Institut d'Oncologia (VHIO)- Edifici Cellex
Barcelona 08035, Spain

2. Results and Discussion

2.1. Preparation and Physicochemical Properties of Quatsomes

With the aim of developing a new nanocarrier for in vitro and in vivo miRNA delivery, different QS formulations were prepared by the DELOS-SUSP process. The membrane components of the new QS included two non-water-soluble sterols, cholesterol (Chol) and/or DC-Chol, at four different molar ratios, and the myristalkonium chloride (MKC), an European Medicines Agency (EMA)-approved derivative of the quaternary ammonium surfactant benzalkonium chloride (BAK,EMA/CHMP/495 737/2013), in pure water (Table S1, Supporting Information, **Figure 1**A). Chol was used in the formulations due to its fusogenic properties[29] and high biocompatibility with cellular membranes.[30] DC-Chol was introduced into QS in order to confer an ionizable pH-sensitive behavior owing to the presence of a tertiary amine group at the end of the hydrophobic chain. The cationic MKC surfactant was used for assembly with the sterol molecules, which induces nanovesicle formation.[21] The capacity of these nanovesicles to electrostatically interact and form complexes with negatively-charged molecules like sRNAs (e.g., miRNA, siRNA), is given by the permanent positive charges of MKC and the protonated tertiary amines of DC-Chol.

Four QS formulations named QS_1, QS_2, QS_3, and QS_4 were prepared, with constant quantities of MKC but varying amounts of Chol and DC-Chol. Indeed, the amount of DC-Chol increased from QS_1, with no DC-Chol and the highest amount of Chol, to QS_4, with no Chol and the highest amount of DC-Chol (Figure 1A and Table S1, Supporting Information).

The size distribution and surface charge indicated that all formulations were composed of small vesicles with diameters ranging from 50 to 125 nm (Figure 1B), with a low polydispersity index (PDI, 0.15–0.4, Table S2, Supporting Information, Figure 1C) and positive surface charges (ζ-potential between +80–100 mV, Figure S1A, Supporting Information). All QS formulations had a slightly acidic-neutral pH (pH 6–7, Figure S1B, Supporting Information). Furthermore, QS were stable in terms of size, charge, and pH up to, at least, 6 months (Figure 1B,C and Figure S1A,B, Supporting Information), and QS_3 and QS_4 were stable for even longer than two years (Figure S1C–F, Supporting Information). Cryogenic transmission electron microscopy (cryo-TEM) images showed a highly uniform nanovesicle population with respect to spherical

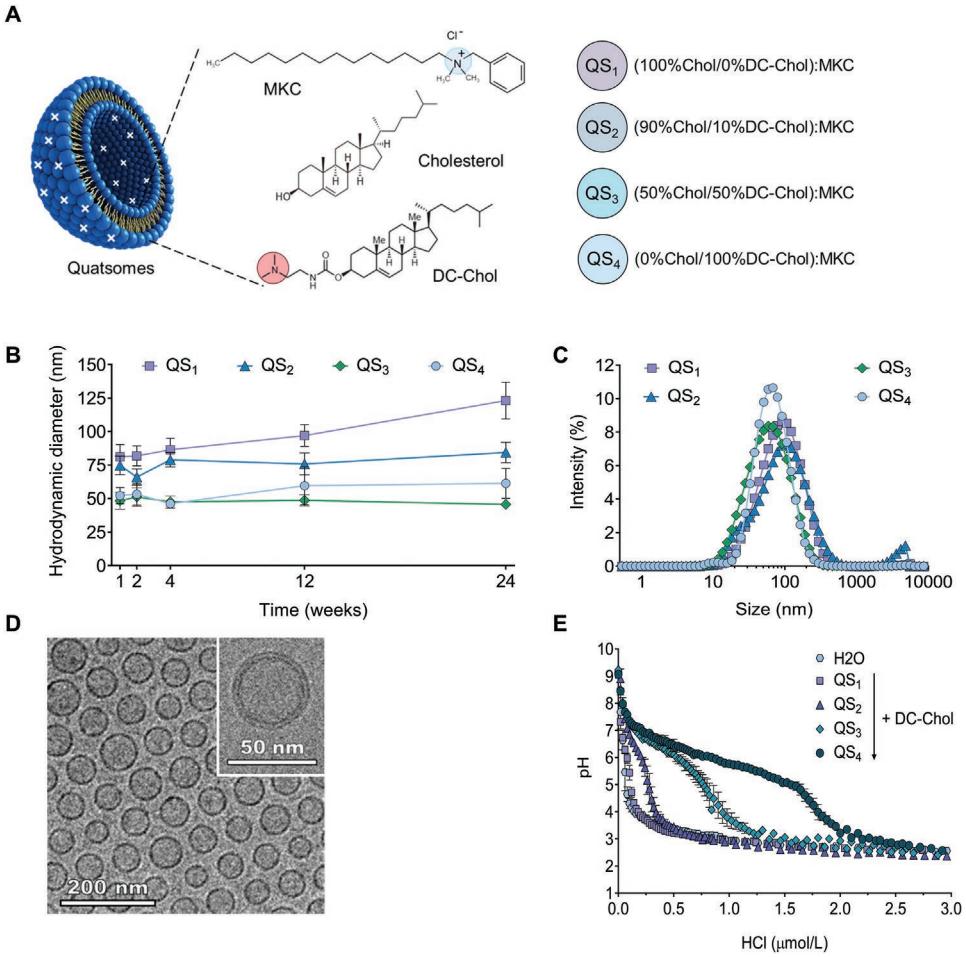

Figure 1. Physicochemical properties of quatsomes. A) Schematic representation of quatsomes (QS) formulations. MKC: Tetradecyldimethylbenzylammonium Chloride, Chol: Cholesterol, DC-Chol: 3β-[*N*-(*N*′,*N*′-dimethylaminoethane)-carbamoyl]cholesterol. B) Temporal evolution of the QS hydrodynamic diameter. C) QS hydrodynamic diameter distribution. Zooming of one nanovescicle showing its bilayered membrane and unilamerality. Graph represents triplicate measurements obtained from different batches of each formulation ± SD. D) Cryo-TEM images of QS_4. E) pH-buffering capacity of the different QS formulations. Graph represents pH variations with an acidic HCl concentration from 0 to 3 µM, values are the average of three independent experiments ± SEM.

morphology and unilamellarity, which confirms that DC-Chol also self-assembles with MKC into nanovesicles (Figure 1D, Figure S2, Supporting Information), as previously reported for Chol:MKC mixtures (QS_1).[21]

The protonation capacity of the different QS formulations was tested. QS_1, which does not contain any protonable tertiary amine, showed a sharp pH decrease upon the addition of small HCl amounts (Figure 1E). On the contrary, QS_2, QS_3, and QS_4, which contain DC-Chol, showed a softer pH decrease upon addition of HCl, proportional to the increasing content of this sterol derivative (Figure 1E). These results indicate that the protonation capacity of our nanovesicles increases progressively as a function of the DC-Chol content, leading to a pH-dependent surface charge density of QS_2, QS_3, and QS_4.

2.2. Complexation of MicroRNA to Quatsomes

To demonstrate the formation of QS-miRNA complexes and determine the loading capacity, for each of the $QS_{1–4}$ formulations, we prepared 8 different QS_X-miRNA complexes by incubation in PBS, at increasing QS_X-miRNA ratios. These complexes were extemporaneously prepared (before use) maintaining the same miRNA concentration but lower concentrations of QS. They are called QS_X-miRNA (Y), where Y is a roman number that represents the loading increase of miRNA per QS (e.g., QS_1-miRNA (I)) (Tables S3 and S4, Supporting Information).

Among the four formulations studied, QS_4 was the most efficient in binding miRNA at the lowest QS concentration used, showing less amount of free miRNA in the electrophoretic agarose gel assay (Figure S3, Supporting Information). The correlation observed between the amount of DC-Chol and miRNA binding efficiency in QS_{2-4} suggests that DC-Chol is a critical component for optimal miRNA complexation. QS-miRNA complexation was also confirmed by the addition of a competing negatively-charged agent such as the unfractioned heparin or the anionic surfactant sodium dodecyl sulfate (SDS) that release the miRNA previously bound to QS (Figure S4, Supporting Information).

The morphologies of the QS-miRNA complexes were analyzed by cryo-TEM (Figure S5, Supporting Information). When

DC-Chol in the membrane was absent or at low content ($QS_{1,2}$), QS maintained the vesicular structure but formed concentric, densely packed, multi-layer assemblies with miRNAs. On the other hand, complexes with higher amounts of DC-Chol ($QS_{3,4}$) exhibited more compact structures with vesicle deformations, and morphological differences and structure complexity that depend on the miRNA loading. At low miRNA loadings per QS_4, that is, QS_4-miRNA (I–III), (Table S4, Supporting Information), assemblies of alternating flattened bilayers and miRNA domains were found, resembling DNA–cationic vesicle assemblies in excess lipid (Figure S5, Supporting Information, left panel).[31–33] When the loading of miRNA was increased, that is, QS_4-miRNA (IV–VI), more compact and dense structures with highly deformed vesicles were observed (Figure S4, Supporting Information, middle panel). Finally, excessive amount of nucleic acids, that is, QS_4-miRNA (VII,VIII), destabilized QS vesicles and induced the formation of large and highly compact multi-domain aggregates (Figure S5, Supporting Information, right panel).[34]

2.3. Study of Quatsomes-MicroRNA Transfection in Neuroblastoma Cells

The in vitro effects of QS-miRNA complexes was studied for QS-miRNA complexes with the highest miRNA complexation, that is, QS_1-miRNA (I–IV), QS_2-miRNA (I–VI), QS_3-miRNA (I–VII), and QS_4-miRNA (I–VIII) (Table S4, Supporting Information).

To demonstrate the transfection capacity, neuroblastoma cells were incubated with complexes formed by $QS_{1\text{-}4}$ and fluorescently labelled control miRNA, and subsequently imaged using confocal microscopy. The miRNA control used has the cel-miR-67 mature sequence of *C. elegans*, which does not have a functional effect on neuroblastoma cells.[28] All $QS_{1\text{-}4}$-miRNA formulations showed a similar internalization capacity than lipoplexes prepared with Lipofectamine 2000 (LF 2000),however, naked miRNA was not internalized (**Figure 2**A). Furthermore, none of the tested QS-miRNA co-localized with lysosomes (or very rarely), suggesting that these complexes are mostly internalized by non-endocytic pathways (Figure 2B), unlike what has been reported for other nanocarriers such as, cationic liposomes, lipid NPs, polymeric NPs, and silica-based NPs.[35–37] For further QS-miRNA functional studies we selected miR-323a-5p due to its tumor-suppressive potential in neuroblastoma.[28] LF 2000-miR-323a-5p or $QS_{1\text{-}4}$-miR-323a-5p complexes were incubated with the SK-N-BE(2) neuroblastoma cell line and miR-323a levels were analyzed at 48 h post-transfection by real-time qPCR. In contrast to naked miR-323a-5p, which was unable to enter in neuroblastoma cells, a $\approx 10^3$-fold change increase in miR-323a-5p levels was observed after transfection with $QS_{1\text{-}4}$-miR-323a-5p complexes compared with $QS_{1\text{-}4}$-miR-Control transfected cells, with similar levels to those obtained by LF 2000 transfection (Figure 2C). Of note, the complexation of miR-323a-5p with micelle-like NPs, composed only of MKC, was an unsuccessful strategy to raise intracellular miR-323a-5p levels (Figure S6A, Supporting Information), suggesting that the complete small unilamellar nanovesicular structure of QS is necessary for an efficient miRNAs transfection.

2.4. Biocompatibility of Quatsomes-MicroRNA Complexes

To determine the range of toxicity of QS-miRNA complexes, all samples indicated in the Table S4 of the Supporting Information, were prepared by loading QS with a control miRNA (i.e., Dy547-labelled cel-miR-67), which does not target human sequences and does not impact on cell viability.[28,38] Cell proliferation experiments were evaluated after 24 h of incubation with increasing concentrations of QS-miR-Control complexes or QS alone (Figure 2D and Figure S7, Supporting Information, respectively). None of the QS formulations affected the cell viability at the concentrations needed for an optimal miRNA transfection (i.e., QS-miRNA loadings (IV, V, or VI), which correspond to a range of QS concentrations between 3.0 and 6.4 $\mu g\ mL^{-1}$ depending on the QS formulation (Table S5, Supporting Information).

2.5. Study of QS_4-miR-323a-5p Functional Response

miRNA are key regulators of multiple target genes inducing mRNAs target genes cleavage or translational repression.[39] In previous work, we demonstrated that miR-323a-5p tumor-suppressive effects are mediated, at least in part, by the modulation of cell cycle-related genes such as, cyclin D1 (CCND1) and chromatin assembly factor 1 subunit A (CHAF1A), mRNA levels of which are reduced after restoration of miR-323a-5p levels.[28] Therefore, to determine the functionality of $QS_{1\text{-}4}$-miRNA complexes we analyzed the mRNA and protein levels of such miR-323a-5p target genes. Despite the similar transfection efficacy observed for all QS formulations, different effects on mRNA and protein expression levels were found. Indeed, while QS_4-miR-323a-5p complexes were able to efficiently downregulate CHAF1A and CCND1 at both mRNA and protein levels (**Figure 3**A–E), neither naked miR-323a-5p, nor MKC-miR-323a-5p micellar complexes nor $QS_{1,2}$-miR-323a-5p complexes produced any variations in CCND1 or CHAF1A mRNA (Figure 3A,B, Figure S6B, Supporting Information) or the corresponding protein levels (Figure 3C–E, Figure S6C, Supporting Information). QS_3-miR323a-5p only modified CHAF1A and CCND1 expression minimally. These results suggest that DC-Chol is a critical component of QS, possibly facilitating miRNA release through a pH-triggered deprotonation.

To characterize how miRNAs are released from QS upon cell internalization, we monitored the QS-miRNA complexation/decomplexation using fluorescence resonance energy transfer (FRET). QS and miRNA were each labelled with a fluorophore that together form a FRET pair: QS were labelled with DiI, which acts as the donor, while miRNA was labelled with Cy5, which acts as the acceptor (**Figure 4**A and Figure S9A, Supporting Information). Importantly, the presence of the fluorophore did not alter the physicochemical properties of QS (Figure S8A–E, Supporting Information) or the miRNA complexation efficiency (Figure S8F, Supporting Information). ^{DiI}QS-miR-Control^{Cy5} complexes, when excited at 550 nm, showed a strong emission of the acceptor dye Cy5 due to the FRET effect (Figure 4B and Figure S9B–E, Supporting Information), while QS-miRNA complexes labelled with only one fluorophore (blue line in Figure 4B), did not cause the direct excitation of Cy5.

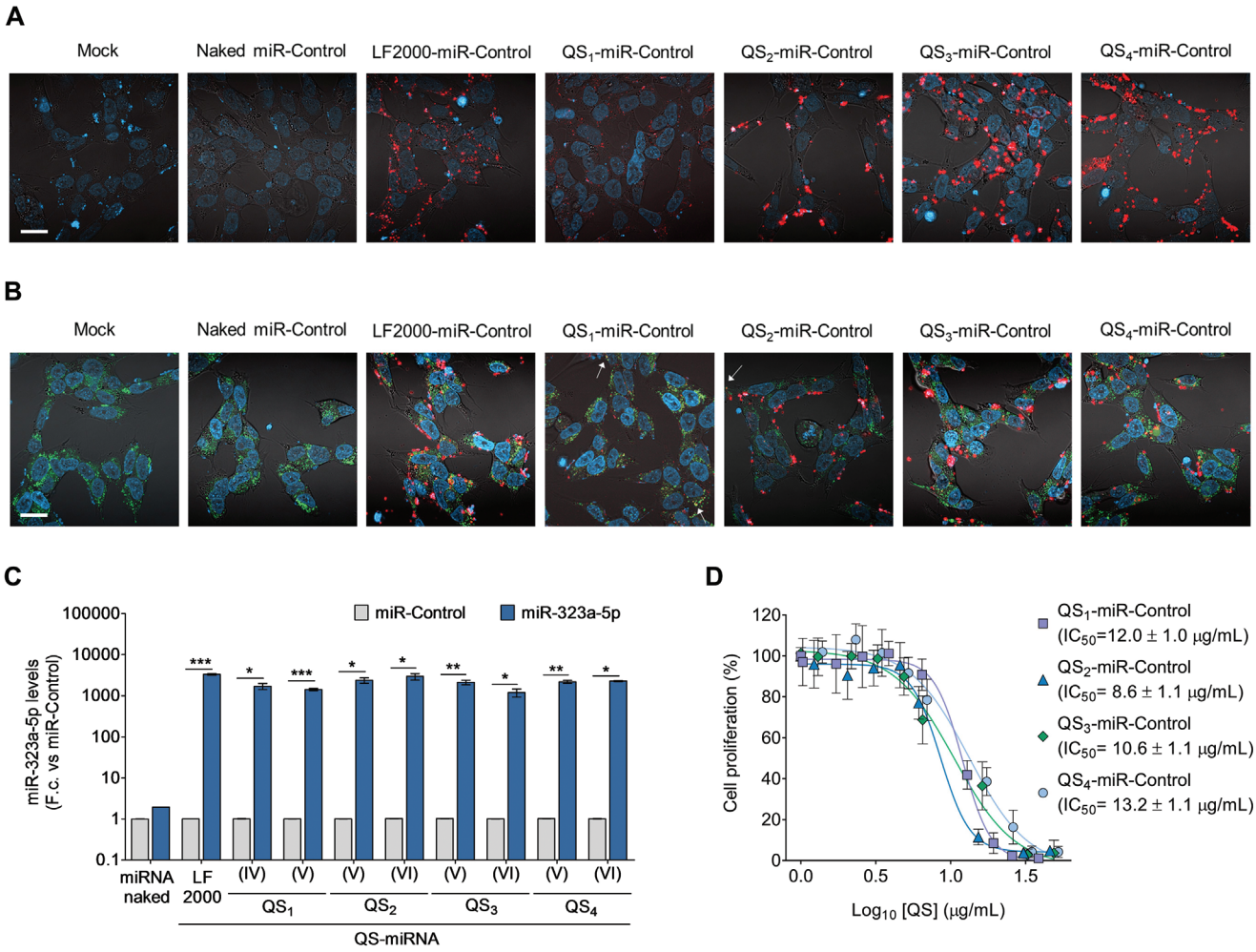

Figure 2. QS-miRNA complexes are efficiently internalized in neuroblastoma cells. A) Representative confocal images of non-transfected (Mock) neuroblastoma cells or incubated for 24 h with naked Dy547 -labelled miR-Control (red staining), complexed with Lipofectamine 2000 (LF 2000) or the $QS_{1\text{-}4}$ formulations. Nuclei were stained with 4',6-diamidino-2-phenylindole (DAPI) and acquired images were superposed with bright field. Scale bar represents 20 μm. B) Lysosome co-localization analyses with the above-indicated conditions. Lysosomes were stained using Lysotracker Green. White arrows point at miRNA-lysosome co-localization events. Nuclei were stained with 4',6-diamidino-2-phenylindole (DAPI). Scale bar, 20 μm. C) MiRNA levels in SK-N-BE(2) cells transfected with miR-Control or miR-323-5p with the indicated formulations measured by qPCR using Lipofectamine 2000 (LF 2000) or with the indicated QS_x-miRNA (Y) ratios, where X is the number of QS system (1-4) and Y is a roman number that represents the loading increase of miRNA per QS (e.g., QS_1-miRNA (I)) (Tables S3 and S4, Supporting Information). miRNA levels were normalized to RNU-44. F.c. means fold change of miR-323a-5p versus miR-Control. Graph represents the mean of three independent experiments ± SEM. * $p < 0.05$,** $p < 0.01$,*** $p < 0.001$. D) Cell proliferation of SK-N-BE(2) cells treated with $QS_{1\text{-}4}$-miR-control complexes at different QS-miRNA concentrations. Graph Represents the average of three independent experiments ± SEM.

Importantly, the decomplexation of the $^{DiI}QS_4$-miR-Control^{Cy5} complex with the anionic surfactant SDS led to a significant reduction of the FRET signal, owing to the increased distance between the labelled miRNA^{Cy5} and $^{DiI}QS_4$. To demonstrate qualitatively the different sensitivity of QS_1-miRNA and QS_4-miRNA toward the variation of pH, we incubated the FRET-labelled QS-miRNA complexes in buffers with different pH. $^{DiI}QS_1$-miR-Control^{Cy5} exhibited an unchanged FRET efficiency over the whole pH range (Figure 4C, grey dots), indicating that a pH increase does not provoke the miRNA detachment. In contrast, in alkaline pH (>7.2) $^{DiI}QS_4$-miR-Control^{Cy5} showed a FRET ratio decrease (Figure 4C, blue dot), provoked by the release of miRNA due to the deprotonation of the tertiary amines of DC-Chol. This deprotonation was confirmed by the abrupt decrease of the cationic surface charge density of QS_4 at a pH-range between of 7.2 and 8.2 (see Figure S9F, Supporting Information).

Next, FRET-labelled QS-miRNA complexes were transfected in live SK-N-BE(2) cells. As observed in Figure 4D–G, we found very significant differences in FRET ratio among the distinct ^{DiI}QS-miR-Control^{Cy5} formulations. QS_1 and QS_2 formulations did not show an apparent release of miRNA, since no change in FRET ratio was observed up to 12 h post-transfection (Figure 4D,E). However, QS_3 showed a progressive but modest release of miRNA (Figure 4F) and QS_4 complexes displayed a much faster and pronounced reduction of FRET ratio, thereby indicating an efficient release of miRNA (Figure 4G). A representative image of $^{DiI}QS_4$-miR-Control^{Cy5} complexes 2.5 h

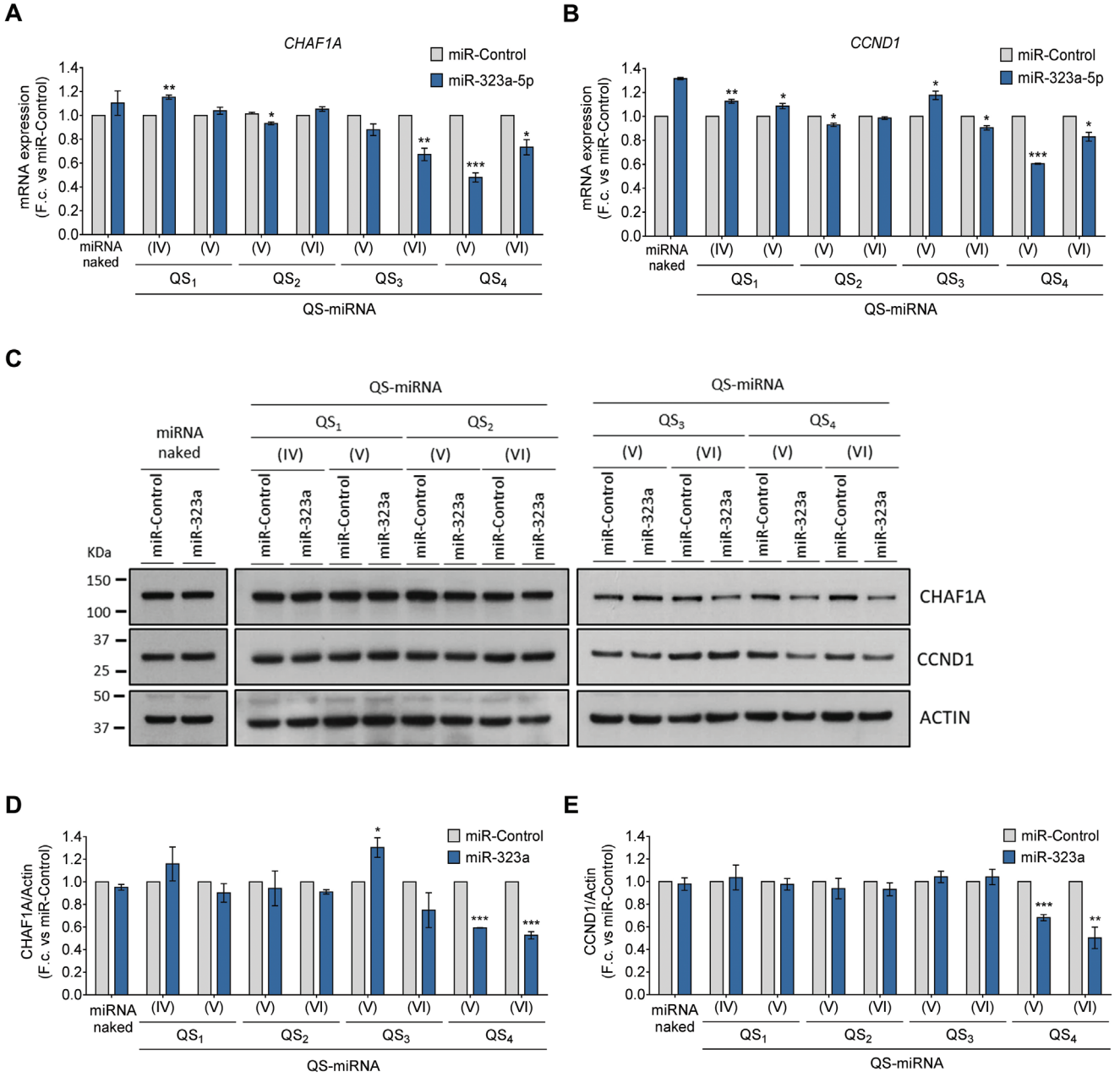

Figure 3. QS_4-miR-323a-5p complexes modulate miR-323a-5p targets at mRNA and protein level. A,B) Gene expression analysis of CCND1 and CHAF1A 48 h post QS-miR-323a-5p (blue bars) or QS-miR-Control (grey bars) transfection, measured by qPCR. F.c. means fold change. Graph represents the mean of three independent experiments ± SEM. C) Western blot of the indicated proteins after transfection of neuroblastoma cells with 50 nM of miR-control or miR-323a-5p for 48 h. D,E) Histograms represent the quantification of band intensity from western blots shown in C. Protein levels were normalized versus actin and represented as the average of three independent experiments ± SEM. A.u. means arbitrary units. * $p < 0.05$,** $p < 0.01$,*** $p < 0.001$.

post-transfection is shown in Figure 4H, demonstrating a large fraction of destabilized complexes (i.e., low FRET efficiency).

DiI fluorophore is a lipophilic carbocyanine insoluble in water that lose their fluorescence when dispersed in aqueous media. As previously reported, DiI labelled QS do not lose their fluorescence upon cellular internalization, thereby indicating that this dye remains attached to QS.[23] Overall, monitoring the FRET efficiency offers a valuable tool to assess the complexation state in space and time in vitro and during cell uptake and trafficking.

These results correlate well with the observed degree of miR-323a-5p target's modulation by the different QS-miR-323a-5p formulations in Figure 3. Thus, we demonstrate that the miRNA-induced functional response is only achieved when miRNAs are released from the complexes, which is mainly observed for QS_4-miRNA. Our results support the hypothesis that miRNA remains complexed with QS_4 in the acidic extracellular media and is released from QS_4 in tumoral cells, which have been described to have a higher intracellular pH (pH > 7.2) than healthy cells.[40–44]

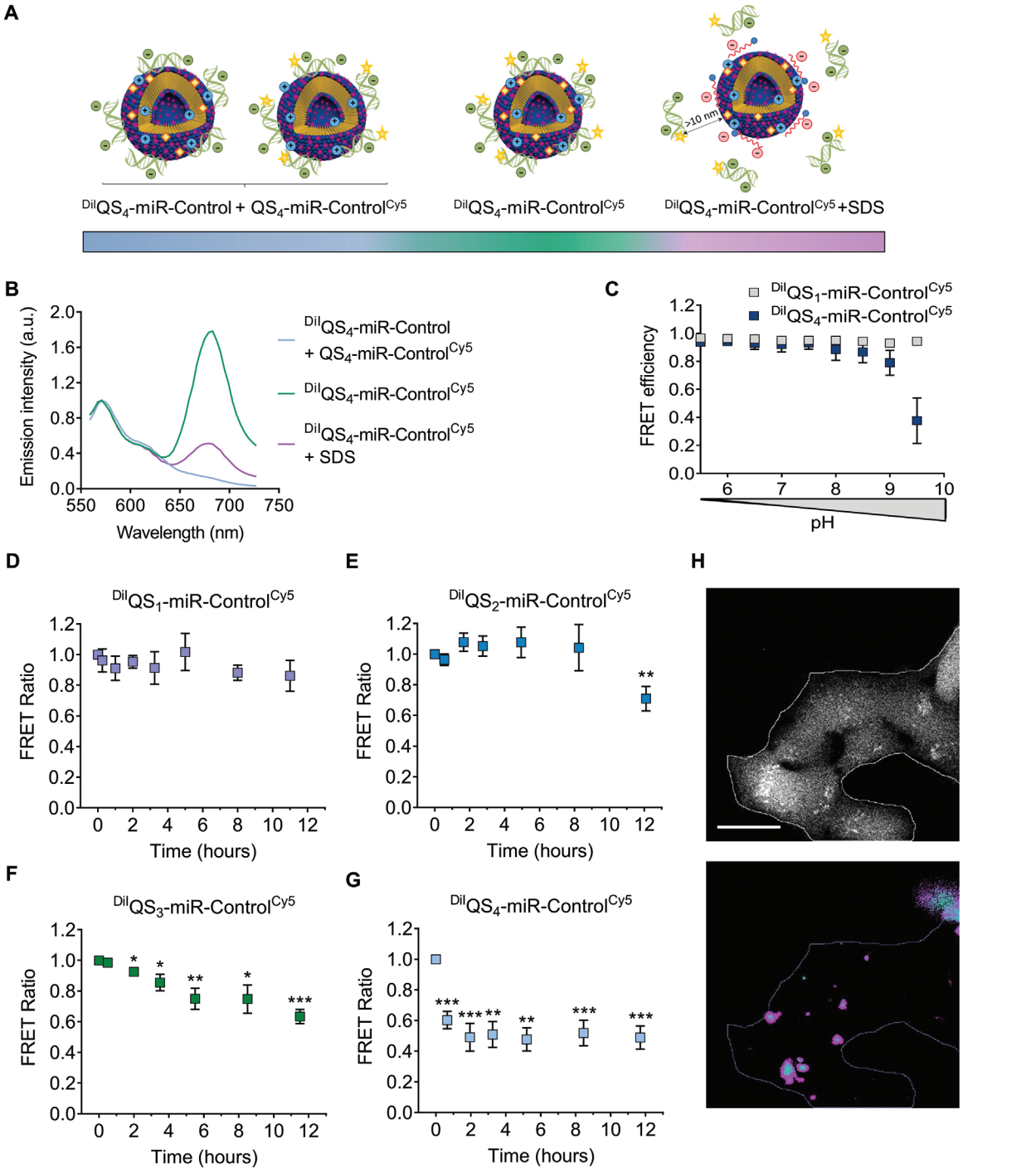

Figure 4. Analysis of QS-miRNA dynamics by FRET. A) Schematic representation of the $^{DiI}QS_4$-miR-Control^{Cy5} FRET systems. FRET only occurs (green signal) in the middle panel, when labelled QS and miRNA are in close proximity (<10 nm). FRET is absent in the left panel, when only one of the components of the QS-miRNA complex is labelled. FRET is also lost (pink signal, right panel) when labelled QS-miRNA complexes are disrupted with SDS. B) Emission spectra of complexes prepared with Cy5 labelled miRNA and QS_4 loaded with DiI. The $^{DiI}QS_4$-miR-Control^{Cy5} system (green) corresponds to the complexes with both miR-Control labelled with Cy5 and QS_4 labelled with DiI. The blue spectra correspond to the addition of the spectra of $^{DiI}QS_4$-miR-Control (non-labelled miRNA) plus the spectra of QS_4-miR-Control^{Cy5} (non-labelled QS). After the addition of SDS the spectra (pink) of $^{DiI}QS_4$-miR-Control^{Cy5} system was observed. The emission spectra of ^{DiI}QS-miR-Control^{Cy5} were normalized with respect to the maximum intensity of the donor (DiI) to monitor the variation in relative intensity of the acceptor (Cy5). C) FRET efficiency comparing $^{DiI}QS_1$-miR-Control^{Cy5} with $^{DiI}QS_4$-miR-Control^{Cy5} in different buffers in a range of pH from 5 to 9.5. D–G) FRET ratio ($I_{miR\text{-}Control^{Cy5}}/I^{DiI}QS_4$) of ^{DiI}QS-miR-Control^{Cy5} complexes over time with the different QS formulations after overnight transfection in SK-N-BE(2) neuroblastoma cells. Values were represented as the average of nine independent measures ± SEM. The statistical comparison is between the FRET ratio at time 0 h (control) versus each of the other time points analyzed. * $p < 0.05$,** $p < 0.01$,*** $p < 0.001$. H) Representative image of FRET confocal analysis of $^{DiI}QS_4$-miR-Control^{Cy5} complexes (right) 14 h post-transfection.

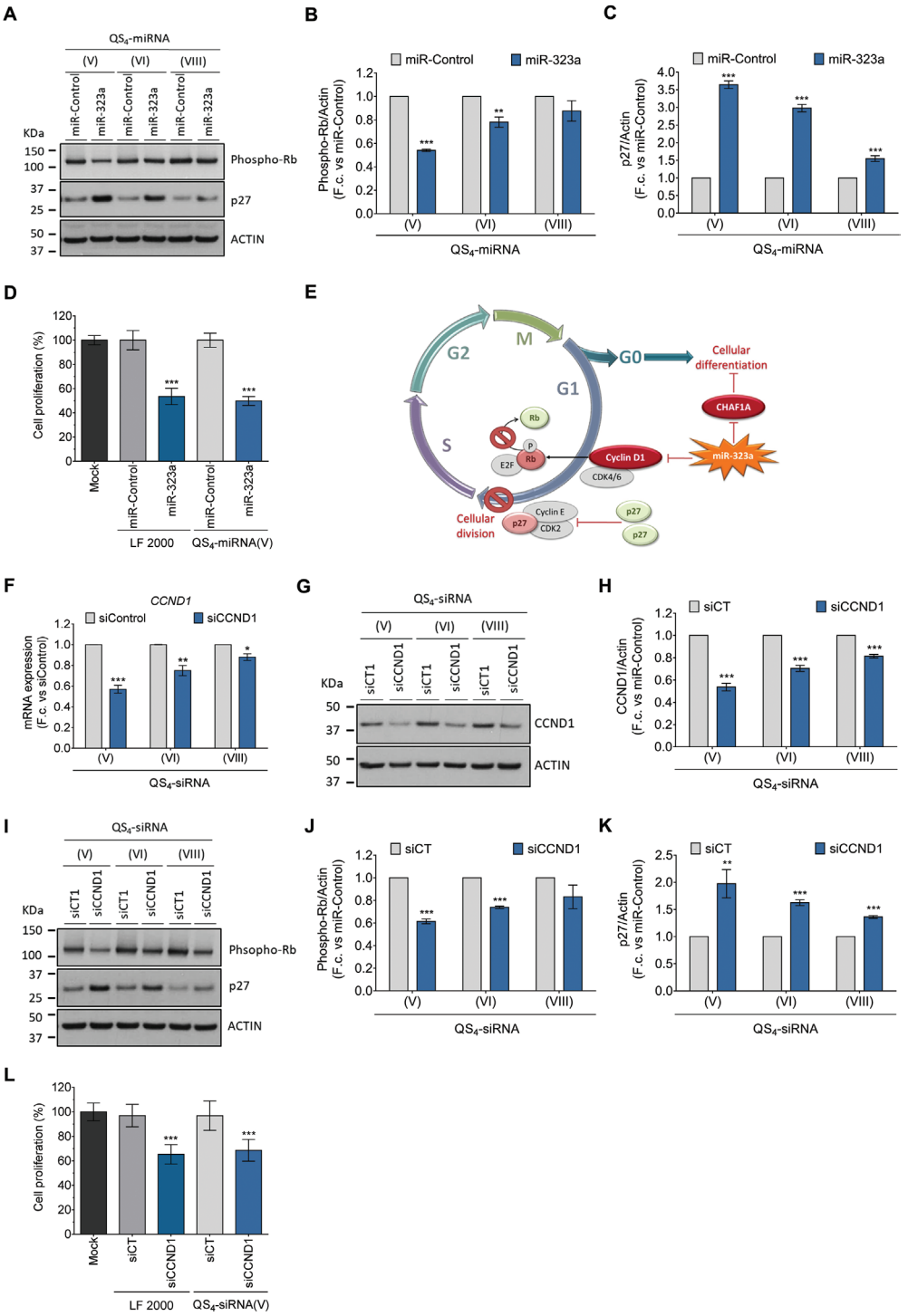

Figure 5. QS_4-miR-323a-5p and QS_4-siCCND1 complexes elicit a molecular and functional response in neuroblastoma cells. A) Representative western blot of the indicated proteins after transfection of QS_4-miR-Control or QS_4-miR-323a-5p complexes in SK-N-BE(2) cells. Loadings V, VI, and VII represents increasing ratio of miRNA per QS. B,C) Graphs represents the quantification of band intensity of from (A). D) Cell proliferation experiment of SK-N-BE(2) using Lipofectamine 2000 (LF 2000) or QS_4 to transfect miR-323a-5p or miR-Control at 96 h post-transfection. E) Schematic illustration of miR-323a-5p regulation of cell proliferation and differentiation in neuroblastoma. F) qPCR CCND1 mRNA expression analysis of SK-N-BE(2) cells transfected with QS_4-siCCND1 complexes for 48 h. F.c. means fold change of miR-323a-5p versus miR-Control. G) Representative western blot of SK-N-BE(2) cells transfected with QS_4-siCT (non-silencing control) or siCCND1 for 48 h. H) Band intensity quantification of (G). Graph represents the average of three experiments ± SEM. I) Representative western blot of SK-N-BE(2) cells transfected with QS_4-siCT (non-silencing control) or siCCND1 for 72 h. J,K) Band intensity quantification of (I). Graph represents the average of three experiments ± SEM. Expression values are normalized versus actin. L) Cell proliferation experiment at of SK-N-BE(2) cells using Lipofectamine 2000 (LF 2000) or QS_4 to transfect siRNA-Control or siCCND1 for 96 h. * $p < 0.05$,** $p < 0.01$,*** $p < 0.001$.

2.6. Use of QS_4-miR-323a-5p Complexes for Halting the Proliferation of Neuroblastoma Cells

In basal conditions, CCND1 interacts with CDK4 and CDK6, thereby activating the complex and inducing the phosphorylation of Rb, which becomes activated and permits cell cycle progression.[45] If CCND1 levels fall, for example due to inhibition by miR-323a-5p, Rb phosphorylation is reduced and cell cycle progression is halted. Therefore, the cell cycle inhibitor p27 levels are increased (**Figure 5**A–C,E).[28,46] When neuroblastoma cells were incubated with QS_4-miR-323a-5p for 72 h, a reduction in the phosphorylation of Rb was observed with a concomitant upregulation of the cell cycle inhibitor p27 (Figure 5A–C). Concurring with these molecular observations, cell proliferation was also reduced, with similar effects compared to LF 2000 lipoplexes (Figure 5D). As expected, naked miR-323a-5p or conjugated to MKC micelle NPs did not alter Rb phosphorylation or p27 accumulation (Figure S6D,E, Supporting Information).

To ascertain whether QS_4 could be used to deliver other sRNAs, we proceeded to complex QS_4 with a siRNA control (siCT) or with siRNA against CCND1 (siCCND1) and transfect them into SK-N-BE(2) cells (Table S4, Supporting Information). 48 h post-transfection, QS_4-siCCND1 was able to reduce CCND1 at mRNA and protein levels (Figure 5F–H). Similarly, QS_4-siCCND1 complexes blocked Rb phosphorylation, p27 accumulation, and reduced neuroblastoma cell proliferation (Figure 5I–L).

In summary, our data indicates that QS_4 nanovesicles are an efficient strategy for the intracellular delivery of tumor-suppressive miRNA and siRNA in neuroblastoma.

2.7. QS_4-miRNA Behavior In Vivo

To delve into the QS_4-sRNA complexes behavior in vivo, the stability of QS_4-miR-323a-5p complexes was studied in presence of serum. The incubation of QS-miRNA complexes with serum did not alter the binding of miR-323a-5p to QS_4 (Figure S10, Supporting Information), demonstrating their stability in complex fluids.

Several studies reported that naked miRNA presents a short half-life after in vivo administration owing to nuclease degradation.[47,48] Therefore, to test the integrity of the miR-323a-5p in our nanoformulation, QS_4-miR-323a-5p complexes were incubated with 25 µg mL^{-1} of RNAse A, a ribonuclease capable of degrading sRNAs.[36] While naked miR-323a-5p was clearly processed after 30 min of RNAse A incubation, as shown by the evident mobility shift in the agarose gel (**Figure 6**A, lanes 9–12), miRNA released from QS_4-miR-323a-5p complexes with SDS (Figure 6A, lanes 5–8) presented the same size as untreated naked miR-323a-5p (Figure 6A, lanes 13–14) or complexes without RNAse A incubation (Figure 6A, lane 4). These results indicate that miRNA bound to QS are not degraded by RNAses.

Finally, we traced the biodistribution of QS_4-miRNA complexes in vivo. DiI labelled QS_4-miR-323a-5p reduced neuroblastoma cells proliferation compared with plain QS_4 (Figure S11, Supporting Information). $^{DiI}QS_4$ were then conjugated with miR-Control or miR-323a-5p and administered intravenously at 2 mg kg^{-1} into athymic nude-Foxn1nu mice bearing subcutaneous SK-N-BE(2) neuroblastoma xenografts. A single administration of $^{DiI}QS_4$-miRNA complexes was

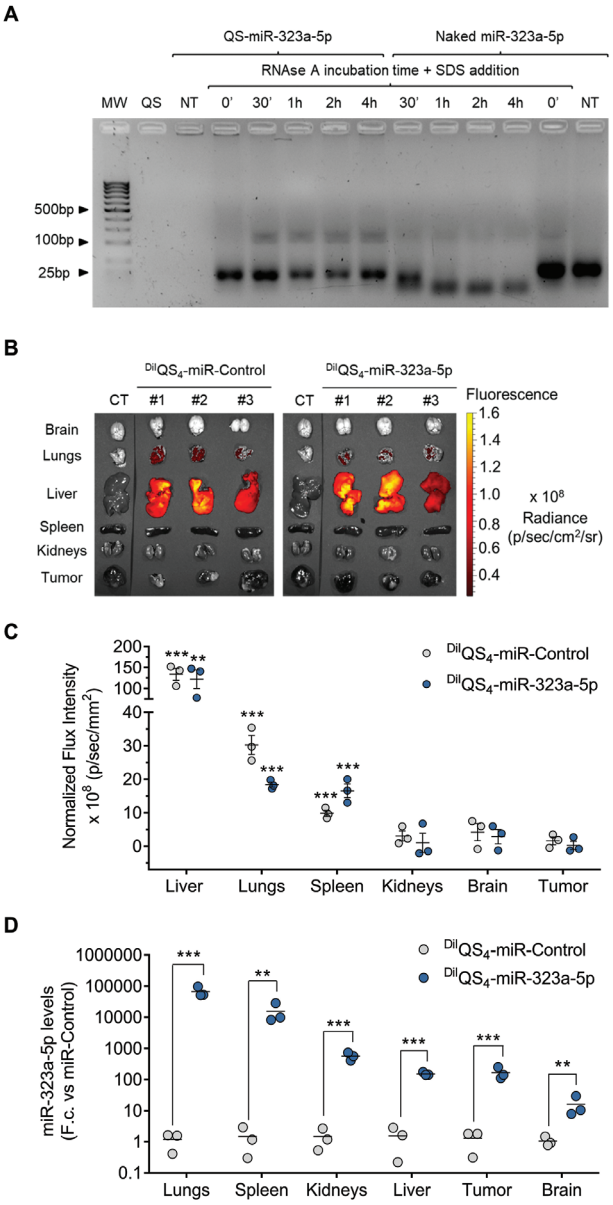

Figure 6. QS_4 protects miRNA from nuclease degradation and increases the miR-323a-5p levels in different mouse organs and neuroblastoma xenografts. A) Nuclease degradation assay. Gel electrophoresis showing QS_4-miR-323a-5p complexes (lanes 5–8) or naked miR-323a-5p (lanes 9–12) treated with 25 µg mL^{-1} RNAse A for the indicated times. SDS-mediated de-complexation was performed at the end of the experiment to visualize the integrity of the complexed miRNA (lanes 4–13). Lanes labelled "NT" are QS_4-miR-323a-5p complexes non-treated with RNAse A and SDS (lanes 3 and 14). These experiments were performed in triplicate. B) QS-miRNA biodistribution analysis. Ex vivo DiI fluorescence imaging of brain, lungs, liver, spleen, kidney, and tumor 24 h post intravenous administration of $^{DiI}QS_4$-miR-323a-5p or $^{DiI}QS_4$-miR-Control complexes. The spectrum gradient bar corresponds to the epifluorescence intensity in radiance unit (p sec^{-1} cm^{-2} sr^{-1}). C) Quantification of the mean fluorescence intensity of the DiI signal of excised organs (n = 3/group) shown in B). Graph represent as the mean fluorescence of each organ from three different animals ± SEM. D) Relative miR-323a levels, of the indicated tissues measured by qPCR. F.c. means fold change of miR-323a-5p versus miR-Control. * $p < 0.05$,** $p < 0.01$,*** $p < 0.001$.

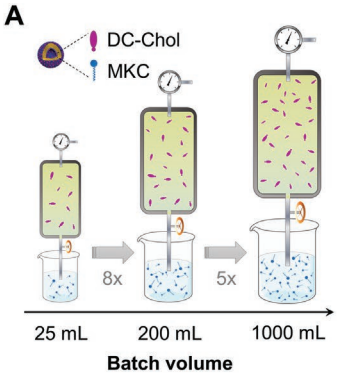

B

Batch volume	Hydrodynamic diameter (nm)	PDI	ζ-potential (mV)	pH
25 mL	52.1 ± 0.4	0.29 ± 0.04	87 ± 5	6.2
200 mL	59.1 ± 0.2	0.27 ± 0.04	74 ± 7	6.1
1000 mL	43.3 ± 0.2	0.22 ± 0.01	82 ± 3	6.4

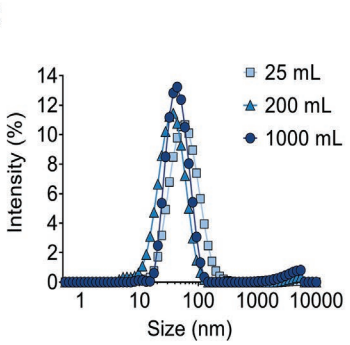

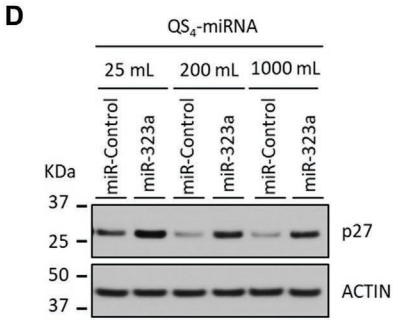

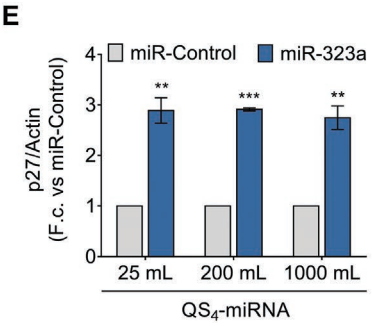

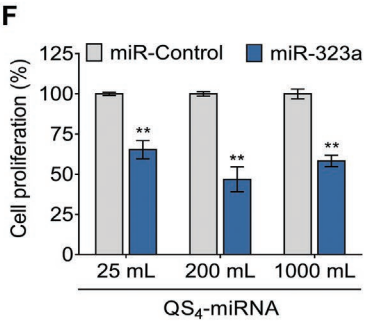

Figure 7. Physicochemical properties and functionality of scaled-up QS4 are similar to QS4 produced at laboratory scale. A) Representation of the scalable QS_4 production by DELOS-susp method. B) Hydrodynamic diameter, PDI, surface charge density, and pH of QS_4 produced in a final batch volume of 25, 200, and 1000 mL. Results are represented as the mean ± SD of three independent measures. C) Hydrodynamic diameter distribution of QS_4 prepared at different batch scales (25, 200, and 1000 mL). D) Representative western blot of the indicated proteins after SK-N-BE(2) cell transfection with QS_4-miR-Control or QS_4-miR-323a-5p complexes using the batches of 25, 200, and 1000 mL. E) Band intensity quantification of (D). Graph represents the average of three experiments ± SEM. Results are represented as the mean ± SD of three independent measures. * $p < 0.05$,** $p < 0.01$,*** $p < 0.001$. F) Cell proliferation experiment in SK-N-BE(2) cells treated with QS_4-miRNA conjugates with batches of 25, 200, and 1000 mL comparing QS-miR-Control versus QS-miR-323a-5p. * $p < 0.05$,** $p < 0.01$,*** $p < 0.001$.

well-tolerated and adverse side effects were not observed up to 24 h post-administration. Ex vivo fluorescence images taken 24 h post-injection showed that QS-miRNA complexes were accumulated mainly in liver, lungs, and spleen (Figure 6B,C). Concurring with these observations, higher miR-323a-5p levels were detected in these tissues (a 150-, 66 000-, and 15 000-fold increase in relation to QS-miRNA control in liver, lungs, and spleen, respectively). Remarkable levels were also observed in other organs such as kidney or in subcutaneous tumors (570- and 125-fold increase in relation to QS-miRNA control, respectively, Figure 6D). This biodistribution pattern is similar to other liposomal nanoparticles,[49,50] with the exception of the lung tropism, which is often restricted to cationic polymers or liposomes with protonable amines.[51,52] Accumulation of QS_4-miRNA complexes in lungs could be due to the DC-Chol recognition by mannose receptors present in lung cells.[53] These results suggest that QS_4-miRNA complexes will be useful not only to deliver miRNAs at the primary tumor site but also to neuroblastoma metastatic sites such as liver or lungs.

2.8. Physico-Chemical and Functional Analysis of Scaled-Up QS_4

To evaluate the scalability of QS_4 production required for in vivo preclinical and clinical studies, QS_4 were prepared in larger high pressure equipment using the DELOS-SUSP method, yielding final batch sizes of 25, 200, and 1000 mL (**Figure 7**A). QS_4 prepared at a final batch volume of 200 and 1000 mL had similar physicochemical properties to those obtained at the lowest laboratory scale (25 mL), in terms of particle size distribution (Figure 7B), hydrodynamic diameters, PDI, ζ-potential, and pH (Figure 7C). The different QS_4-miR-323a-5p productions also showed an identical capacity to modulate miR-323a-5p targets (Figure 7D,E) and to inhibit cell proliferation (Figure 7F).

In summary, the production of QS at different scales using DELOS-SUSP showed that QS_4 maintained the same physicochemical properties in terms of size, morphology and functionality, ensuring high vesicle homogeneity and batch-to-batch reproducibility at least up to 40-fold scale-up. This methodology thus allows to overcome the scale-up limitation of a wide range of nanoparticles using a simple, rapid, and green method for the clinical production of nanomedicines.

3. Conclusions

A new type of stable pH-sensitive nanovesicles, based on quatsomes, was developed for delivery of miRNA. The cationic character and pH-sensitive behavior of these non-liposomal

nanovesicles can be finely adjusted by changing their membrane composition, in particular the DC-Chol content, with otherwise minimal alterations in their physico-chemical properties. QS nanocarriers are stable upon storage, preserving their morphology (unilamellar), size (<150 nm), and low polidispersity (<0.25), at least up to 6 months. The control of the pH-sensitivity, through the DC-content in Quatsome membrane, ensures the fine-tuning of these nanovesicles to deliver miRNA or other sRNA with therapeutic function. Indeed, sRNA release was largely dependent on the DC-Chol content, and therewith the differential molecular and functional response. Quatsomes protected miRNA from degradation by nucleases present in the serum, thereby enabling longer circulation time in the blood. When administered intravenously, QS-miRNA complexes were well tolerated and reached subcutaneous neuroblastoma xenograft tumors as well as different organs such as, lung or liver. Furthermore, these miRNA nanocarriers are produced by a one-step, green, scalable and GMP compliant nanovesicle manufacturing procedure,[20,54] which will favor their effective translation to the clinical phases. The high stability of the new pH-sensitive QS, together with its robust manufacturing procedure, make these sRNA nanocarriers attractive compared to other particles with non-demonstrated stability and with multistep and challenging scalability. In conclusion, the pH-sensitive QS reported here constitute a new nanomaterial platform for delivering small RNA in vitro and in vivo and have the potential to be used for the treatment of high-risk neuroblastoma, and also other cancers or human diseases.

4. Experimental Section

Materials: Cholesten-3β-ol (Chol, purity 95%,#A0807,CAS: 57-88-5) and sodium hydroxide (NaOH, purity ≥98%) were obtained from PanReac (Castellar del Vallès, Spain). Cholesteryl *N*-(2-dimethylaminoethyl) carbamate (DC-Chol, purity ≥ 98%,#92 243,CAS: 137056-72-5) and sodium acetate were purchased from Sigma-Aldrich (Saint Louis, Missouri, USA). Benzyldimethyltetradecylammonium chloride (MKC, purity ≥ 99%, #262 393, CAS: 139-08-2) was supplied by AttendBio Research SL (Santa Coloma de Gramenet, Spain). 1,1'-dioctadecyl-3,3,3',3'-tetramethyl-indocarbocyanine perchlorate (DiI,#D-282), was purchased from Life Technologies (Carlsbad, USA). Tris and BIS-Tris were supplied by Santa Cruz Biotechnology. Ethanol was purchased from Teknochroma (Sant Cugat del Vallès, Spain). Carbon dioxide (purity 99.9%) was acquired from Carburos Metálicos S.A. (Cornellà de Llobregat, Spain). All chemicals were used without further purification and all solutions were prepared using pre-treated Milli-Q water (Millipore Ibérica, Madrid, Spain). Human synthetic miRNA mimics, miR-Control-1 (#CN-001000-01), Dy547 labelled-miR-Control-1 (#CP-004500-01), and Cy5 labelled-miR-Control-1 (custom designed from sequence UCACAACCUCCUAGAAAGAGUAGA) and hsa-miR-323a-5p (#C-301085-01) were acquired from Dharmacon Inc. (Lafayette, Colorado, USA). Control siRNA (5' GUAAGACACGACUUAUCGC 3') and siCCND1 (5' CCUACGAUACGCUACUAUAUU 3') were purchased from Sigma.

Quatsomes Preparation: Quatsomes (QS) were composed of sterols, such as, Chol and/or DC-Chol, and quaternary ammonium surfactants with high positive charge such as, benzyldimethyltetradecylammonium chloride (also called Myristalkonium chloride). Different QS were prepared by adjusting the ratio between Chol and DC-Chol components: QS_1: (100%Chol/0%DC-Chol):MKC, QS_2: (90%Chol/10%DC-Chol):MKC, QS_3: (50%Chol/50%DC-Chol):MKC, QS_4: (0%Chol/100%DC-Chol):MKC. All QS were prepared at a molar ratio 1:1 between the different sterols and the MKC surfactant, except QS_1 which was prepared at a 1:3 molar ratio for in vitro experiments. Furthermore, to perform FRET experiments, QS were functionalized with the DiI fluorophore. These QS were called $^{DiI}QS_1$, $^{DiI}QS_2$, $^{DiI}QS_3$, and $^{DiI}QS_4$ and were prepared at Chol/DC-Chol molar ratios mentioned and a molar ratio 1:1 between the different sterols and the MKC surfactant.

QS were prepared using the depressurization on an expanded liquid organic solution-suspension (DELOS-SUSP) methodology.[18] Briefly, a mixture of sterols (Table S1, Supporting Information), such as, Chol and/or DC-Chol, was dissolved in 2.88 mL of EtOH at a temperature of 313–318 K for 10 min. In case of DiI labelled QS, DiI at 1.1×10^{-3} M was added in the organic solution after sterols dissolution. The organic phase then was added to a high-pressure vessel ($V = 7.05$ mL) in which, after 5 min of equilibration at 311 K, supercritical CO_2 was added until the working pressure ($P_w = 11.5$ MPa) was reached, thereby yielding an expanded liquid ethanol solution with a molar CO_2 fraction of 0.60. The vessel was maintained at the working pressure and temperature for 1 h to ensure homogenization of the organic mixture in one-phase inside the reactor. Finally, for vesicle formation, the organic solution was depressurized at 11.5 MPa of N_2 over an aqueous phase at ambient pressure which contained the surfactant MKC dissolved in 24 mL of water, except for QS_1 and $^{DiI}QS_1$ where it was necessary the presence of PBS at 100 mM in the aqueous phase, due to the non-desired precipitation when pure water is used (Table S1, Supporting Information).[23,24] This methodology permitted the preparation of lipid non-liposomal nanovesicles with increasing DC-Chol/Chol ratio with spherical, unilamellar, and homogeneous shapes.

After 1 week of stabilization at ambient conditions, all samples were purified by diafiltration using the KrosFlo Research Iii TFF System (Spectrum Labs from Repligen Corporation, Waltham, Massachusetts, USA). Samples were diafiltered using a size-exclusion mPEs Micro Kros filter column (100 kDa molecular weight cut-off and a surface area of 20 cm^2) to remove ethanol and the excess of non-encapsulated material.

After purification, QS concentration was measured by gravimetric analysis after freeze-drying and the concentrations obtained were 1.35 mg mL^{-1} for QS_1, 2.66 mg mL^{-1} for QS_2, 3.13 mg mL^{-1} for QS_3, and 2.81 mg mL^{-1} for QS_4.

Dynamic Light Scattering and Zeta-Potential Measurements: Particle size, polydispersity, and surface charge density of QS were evaluated by dynamic light scattering (DLS) and electrophoretic light scattering techniques using Zetasizer Nano ZS (Malvern Instruments, Malvern, United Kingdom). The hydrodynamic diameter and PDI were measured using an incident He-Ne laser light of 4 mW, a wavelength of 633 nm and a detector angle fixed at 173° with homodyne detection. Samples were measured as born without modifications or dilution at 298 K. Moreover, the zeta-potential was measured at 298 K with the Zetasizer Nano ZS, using a DTS1070 disposable folded capillary cuvette. Reported values were the average of hydrodynamic diameters ± SD among samples or zeta-potential ± SD. Experiments were carried out at least in triplicate.

QS stability over time was determined by DLS after 1 week, 2 weeks, 1 month, 3 months, and 6 months after sample preparation or purification.

Determination of pH-Sensitive Amines Protonation: The protonation capacity of QS was determined by performing pH titration curves of QS in neutral, slightly acidic, and strong acidic pH. QS were diluted at a final concentration of 5 mg mL^{-1} (total membrane components) in MilliQ treated water. The resulting QS were adjusted at pH 9 with NaOH 0.01 M (Hanna Instruments, Woonsocket, Rhode Island, USA). The titration curve was performed measuring the pH after each addition of 10 µL of HCl (0.01 M) until the pH = 3 was reached. At every point of pH, the hydrodynamic diameter was measured to evaluate the stability of the sample after pH modification. Finally, pH titration curves were plotted as the mean of three experiments ± the SEM of the experiments.

Cryogenic Transmission Electron Microscopy Imaging: Cryo-TEM images were acquired with a JEOL JEM 2011 transmission electron microscope (JEOL, Tokyo, Japan) at 200 kV, or a Tecnai T12 at 120 kV. Samples were placed on a holey carbon grid or a copper grid coated with perforated polymer film before being frozen in liquid ethane. The Gatan 626 holder was used. Images were recorded using a Gatan Ultrascan US1000 CCD camera and analyzed with the Digital Micrograph software.

Quatsomes-Small RNA Complex Formation: QS were diluted in DEPC-treated water (Thermo Fisher Scientific,#750 024) to achieve the desired concentration of 1.13 mg mL^{-1} for QS_1, 1.75 mg mL^{-1} for QS_2, 1.85 mg mL^{-1} for QS_3, and 1.99 mg mL^{-1} for QS_4. To form sRNA and QS complexes, sRNA (2.5 µM) were added over a QS solution at different concentrations depending on the loading of miRNA/siRNA in QS (Tables S3 and S4, Supporting Information). Complexes were diluted in PBS 1X (Fisher,#10 462 372) and incubated during no more than 10 min at room temperature before use. The loading of sRNA in QS, QS-miRNA, or QS-siRNA, was calculated as the ratio between the QS weight and the sRNA weight. Eight loadings of QS-miRNA or QS-siRNA were prepared keeping the sRNA concentration constant and increasing the QS concentration (Table S4, Supporting Information).

Cell Lines: SK-N-BE(2) were acquired from Public Health England Culture Collections (Salisbury, UK) and stored in liquid nitrogen. Upon resuscitation, SK-N-BE(2) cells were cultured in Iscove's modified Dulbecco's Medium (Life Technologies, Thermo Fisher Scientific, Waltham, Massachusetts, USA), supplemented with 10% heat-inactivated fetal bovine serum (FBS) South America Premium, 1% of Insulin-Transferrin-Selenium Supplement (Thermo Fisher Scientific), 100 U mL^{-1} penicillin, 100 µg mL^{-1} streptomycin (Thermo Fisher Scientific), and 5 µg mL^{-1} plasmocin (InvivoGen, San Diego, CA, USA). All cultures were maintained at 37 °C in a saturated atmosphere of 95% air and 5% CO_2. SK-N-BE(2) cells were tested for mycoplasma contamination periodically.

LF 2000-Small RNA Conjugates Formation: The sRNA and LF 2000 conjugates were performed following the manufacturer protocol. Briefly, 8 µL of LF 2000 (Thermo Fisher,# 11 668 019) were mixed with 250 µL of opti-mem (Thermo Fisher,#31 985 070) and incubated it for 5 min. In parallel, 10 µL of sRNA (0.2 nmols) were mixed with 250 µL of opti-mem. After 5 min, the two solutions were combined mixing them gently and incubated 20 min at room temperature. Next, 500 µL of LF 2000-sRNA conjugates were added to 20 cm^2 plates above 3.5 mL of seeded cells without antibiotics.

For proliferation assays, 0.3 µL of LF 2000 were mixed with 25 µL of opti-mem. In parallel, 0.625 µL of sRNA (0.0125 nmols) were mixed with 25 µL of opti-mem. After 20 min of incubation, add 50 µL of LF 2000-sRNA conjugates to 0.3 cm^2 plates above 200 µL of seeded cells.

Confocal Imaging: SK-N-BE(2) cells were seeded at 2×10^4 in 8-wells Ibidi-glass bottom chamber slides 24 h before transfection. Next day, cells were transfected with miR-Control labelled with Dy547 and QS at loading (V) QS-miRNA. After overnight (o/n) incubation cellular media was changed for IMDM supplemented with 10% FBS and antibiotics. Confocal images were acquired using a Leica TCS SP5X microscope. Dy547 was excited using a 559 nm laser. The emitted signal was collected from 570 to 700 nm. Nuclei were stained with 4',6-diamidino-2-phenylindole and was excited using a 353 nm laser. The emitted signal was collected from 410 to 490 nm. Bright field images were obtained using a 405 nm laser wavelenght. For lysosomal co-localization experiments, lysosomes were stained with Lysotracker Green (#L7526,Thermo Fisher Scientific), excited with 500–546 nm laser and collected from 490 to 552 nm, 30 min before QS-miRNA conjugates transfection.

Quantitative Real-Time PCR: Total RNA including sRNAs was extracted from cell pellets using the miRNeasy Mini Kit (Qiagen, Las Matas, Spain). When extracted from tissues, tissues were previously homogenized using the Bead-Ruptor 12 (Omni International, Georgia, USA) homogenizer (20 s at speed 5 mA, two-three cycles until completely homogenization). RNA was reverse transcribed (0.5 µg total RNA) using Taqman RT kit (#4 366 596, Applied Biosystems, Thermo Fisher Scientific), and levels of mature miRNA were quantified using Taqman microRNA assays (#4 440 047, Applied Biosystems, Thermo Fisher Scientific) using 2X Power SYBR Green Master Mix (Applied Biosystems, Thermo Fisher Scientific) and the ABI700SDS equipment. Levels of mature hsa-miR-323a-5p (#0 02695 (MI0000807)) were normalized versus the RNU-44 small RNA (#0 01094 (NR_0 02750)) for in vitro experiments and the U6 small RNA (#0 01973 (NR_0 04394)) for the in vivo experiment. On the other hand, mRNA expression (i.e., CCND1 and CHAF1A) was normalized against L27 ribosomal mRNA (Table S6, Supporting Information). Relative quantification of gene expression was performed with the 2(–ΔΔCt) method.[55]

Cell Proliferation Assays: For cell proliferation experiments, SK-N-BE(2) cells were seeded in 96-well plates at 18×10^3 cells per well or 9×10^3 cells per well (6 replicates/condition) and treated with QS (0.7 µg mL^{-1} to 52 µg mL^{-1}, Table S5, Supporting Information) or reverse transfected with 2.5 µM of miR-Control-Dy547 complexed with QS at the indicated loadings of miRNA in QS (I–IX), to achieve a final miRNA concentration of 50 nM.

24 or 96 h post-transfection, respectively, cells were fixed with 1% glutaraldehyde (Sigma-Aldrich) and stained with 0.5% crystal violet (Sigma-Aldrich). Crystals were dissolved in 15% acetic acid (Fisher Scientific, Hampton, New Hampshire, USA) and absorbance was measured at 590 nm using an Epoch Microplate Spectrophotometer (Biotek, Winooski, VT, USA). The effect of QS-sRNA complexes on cell proliferation was normalized to mock-control-transfected cells.

Fluorescence Resonance Energy Transfer Analysis: The FRET efficiency between ^{DiI}QS and miRNA^{Cy5} was evaluated measuring the emission spectra of QS-miRNA complexes using the microplate reader Infinite 200 PRO (Tecan, Switzerland). Complexes were diluted (1:10) in PBS or IMDM supplemented with 10% of FBS and placed into a 96-well plate (3 replicates per condition). DiI and Cy5 were excited with a wavelength of 530 nm and their spectra was recorded from 560 to 750 nm and 670–750 nm in static conditions.

To study the miRNA release from QS depending on the pH, ^{DiI}QS-miRNA^{Cy5}, QS-miRNA^{Cy5}, and ^{DiI}QS-miRNA complexes were prepared at a final concentration of 2.5 µM of miRNA and 0.26 mg mL^{-1} of QS. Complexes were diluted (1:10) in different pH buffered solutions containing 150 mM NaCl, placed in a 96 black Nunc well-plates (3 replicates per condition, Fisher Scientific). The pH range was covered from 5 to 9.5, using 50 mM of Tris (pH 7.5–9.5), Bis-Tris (pH 5.5–7.5) and sodium acetate (pH 5–5.5). DiI was excited at a wavelength of 490 nm and its spectra were recorded from 510 to 800 nm. As the fluorescence emission of DiI and cy5 varied strongly with pH, the authors did not plot the ratio of their fluorescence emission versus pH. Instead, the FRET efficiency was calculated from the difference of the fluorescence emission intensities of DiI (λ_{em} = 570 nm) in the presence and absence of cy5:

$$E_{FRET} = \frac{I_{DiI} - \left(I_{DiI/cy5} - I_{cy5}\right)}{I_{DiI}} \quad (1)$$

where I_{DiI} is the emission intensity of ^{DiI}QS-miRNA, $I_{DiI/cy5}$ the emission intensity of ^{DiI}QS-miRNA^{Cy5}, and I_{cy5} the emission intensity of QS-miRNA^{Cy5}. To study the pharmacokinetics of QS-miRNA complexes inside neuroblastoma cells, cells were seeded in 8 well Nunc Lab-Tek chamber slides (Thermo Fisher Scientific) 48 h before the assay. Cells were incubated with complexes for 30 min and then the media was replaced to remove the non-internalized complexes. Confocal images were acquired using the LSM 800 microscope (Zeiss, Germany). Bright field images were obtained using a 488 nm laser. DiI and Cy5 were excited using a 530 and 633 nm laser respectively and their signal collected from 550 to 620 nm and Cy5 from 640 to 750 nm, respectively. DiI and Cy5 signals were acquired in two different channels and processed to remove the cross-talk signal. Images of complexes were processed using Fiji-ImageJ software to obtain the variation of the FRET ratio (calculated by the ratio between the intensity of the acceptor (ImiR-Control^{Cy5}) versus the donor ($I^{DiI}QS_4$)) over time. These experiments were done with technical triplicates in triplicate. For FRET ratio graph, each system was represented as the mean ± SD.

Western Blot: Protein extracts were obtained in RIPA buffer 1X (Thermo Fisher Scientific), supplemented with 1X EDTA-free complete protease inhibitor cocktail (Roche, Sant Cugat del Vallés, Spain). Quantification of protein concentration was determined using Lowry assay (DC protein assay, Bio-Rad). Thirty µg of protein were run in NuPAGE 4–12% Bis-Tris gels during 1 h at 150 V at RT. Gels were transferred to iBlot Gel Transfer Stacks PVDF membranes (Thermo

Fisher Scientific) during 1:30–2 h at 110 V at 4 °C. Membranes were incubated with blocking solution (Tris-buffered saline with Tween-20 (TBS-T) with 5% bovine serum albumin) for 1 h at RT and then incubated overnight at 4 °C with the indicated primary antibodies: anti-CCND1 (1:1000 Cell Signaling,ab134175), anti-CHAF1A (1:1000 Cell Signaling,#5480S), P27 (1:1000 Cell Signaling,#3686), and phospho-Rb (1:1000 Cell Signaling,#8516). Next, membranes were incubated with peroxidase-conjugated secondary antibodies for 1:30 h with anti-rabbit IgG-Peroxidase antibody produced in goat (1:10000, Sigma-Aldrich,#A0545). Anti-actin HRP (1:40000 Santa Cruz,sc-1616) was used as loading control. Membranes were finally developed with EZ-ECL Chemiluminescence detection kit (Biological Industries, Kibbutz Beit-Haemek, Israel). Quantification of western blots were performed with Image J[56] and normalized to the intensity of the corresponding actin (i.e., the loading control). Then, the value of this ratio in the miR-control transfected cells was set to 1. Next, the intensity values of the miR-323a-5p condition was normalized with each miR-Control transfected cells condition. The graph shows the average of these normalized values from three independent experiments ± SEM.

RNAse Degradation Assay: QS-miRNA complexes or naked miRNA were incubated with 25 µg mL^{-1} RNAse A for 30 min, 1, 2, and 4 h and followed by an additional incubation with 0.25% SDS to release miRNAs from QS-miRNA complexes. Next, all samples were run in 2.5% agarose gels. Images were acquired using the Gel Doc XR + System (Biorad, Hercules, California, USA).

Mouse Xenograft: All animal procedures were approved by the ethical committee of Vall d'Hebron Research Institute (protocol number 98.17,experimentation project authorization *n*° 11 009). SK-N-BE(2) cells (5×10^6) were injected into the right flank of 6 to 8 week-old female athymic nude-Foxn1nu mice (n = 3 mice/condition) in 300 µL of PBS:Matrigel (1:1). Tumor volume was measured every 2–3 days. Once tumors were ≈100–200 mm^3, mice were randomized in two groups. Mice were injected with 2 mg kg^{-1} of miR-Control (n = 3) or miR-323a-5p conjugated with $^{DiI}QS_4$ (n = 3). After 24 h, liver, lungs, brain, spleen, kidneys, and tumor were removed and weighted. In vivo fluorescence images were acquired with IVIS Spectrum 24 h post-injection. A region of interest was drawn around each organ and the total radiance (photons/second) was measured using Living Image 4.5 software (PerkinElmer). Total flux radiance was normalized versus the fluorescence captured in fluorescence control mice. These results were plotted as the mean ± SEM of three independent mice.

QS_4 Scalability: The scalability of QS_4 was performed using the DELOS-SUSP methodology in an equipment set-up by Nanomol Technologies SL (WO2006079889). Briefly, a 25 and 100 mL high-pressure vessel was used for QS batch production of 200 and 1000 mL, instead of a 6 mL lab-scale vessel maintaining constant the final concentration of membrane components (6.5 mg mL^{-1}). In order to ensure the homogeneity of nanovesicles, a variable speed stirrer was added in the high-pressure vessel and in the collector where the aqueous phase is placed. Finally, the organic phase is depressurized into the aqueous solution at atmospheric pressure.

After 1 week of stabilization at ambient conditions, the samples obtained at the different scales were purified by diafiltration using the semiautomated crossflow filtration system ÄKTA flux S (Cytiva, Marlborough, Massachusetts, USA). Samples were diafiltered using a size-exclusion mPEs MicroKros filter column (70 kDa molecular weight cut-off and a surface area of 40 cm^2) to remove ethanol and the excess of non-encapsulated material.

Statistical Analysis: Unless otherwise stated, graphs represent the average of three independent experiments ± SEM. Statistical significance was determined by unpaired two-tailed Student's *t*-test (GraphPad Prism Software, USA). * means $p < 0.05$,** $p < 0.01$,*** $p < 0.001$.

Supporting Information

Supporting Information is available from the Wiley Online Library or from the author.

Acknowledgements

The funding was received by Ministerio de Educación, Cultura y Deporte (Grant no. FPU16/01099), Ministerio de Economía, Industria y Competividad (Grants MAT2016-80820-R, MAT2016-80826-R and SAF2016-75241-R), the Ministry of Science and Innovation (MINECO) of Spain through grant PID2019-105622RB-I00, from Instituto de Salud Carlos III (Grant no. CP16/00006, PI17/00564, PI20/00530, DTS20/00018) (Co-funded by European Regional Development Fund/European Social Fund) "Investing in your future"), from the EuroNanoMed II platform through the NanoVax project, from CIBER-BBN through grant TAG-SMARTLY, Joan Petit Foundation, Asociación Matem Lo Bitxo and Asociación Española Contra el Cáncer (Grant no. LABAE18009SEGU), as well as, Generalitat de Catalunya through the Centres de Recerca de Catalunya (CERCA) programme and grant no. 2017-SGR-918, and from Agency for Management of University and Research Grants (AGAUR) (Grant no 2018LLAV0064 and SIFECAT IU68-010017). Furthermore, ICMAB-CSIC acknowledges support from the MINECO through the Severo Ochoa Programme for Centres of Excellence in R&D (SEV-2015-0496 and CEX2019-000917-S). Quatsome production and their physicochemical characterization was performed by the ICTS "NANBIOSIS," more specifically in the Biomaterial Processing and Nanostructuring Unit (U6), Unit of the CIBER in Bioengineering, Biomaterials & Nanomedicne (CIBER-BBN) located at the Institute of Materials Science of Barcelona (ICMAB-CSIC). The authors thank the UAB Microscopy service for their help in recording cryo-TEM images. The authors also thank Mr. Adolfo de Hoyos-Limon for pKa measurements, Ms. Patricia Pérez for her help in in vitro experiments, the members of Laboratory Animal Service Unit of Vall d'Hebron Research Institute for their help in the in vivo experiment. The authors thank Editage (www.editage.com) and Ms. Christine O'Hara for English language correction. The authors acknowledge Biorender.com for allowing the adaptation of their templates. Retrieved from https://app.biorender.com/biorender-templates.

Conflict of Interest

The following authors declare the following financial interests/personal relationships which may be considered as potential competing interests: A.B., A.S., N.S., S.G., J.S.T., J.V., M.F.S., and N.V. are inventors of patent PCT/EP2020/06 3195, which protects the new pH-sensitive nanocarries for nucleic acids delivery. J.V., S.S., and N.V. are further inventors of patent WO2006079889, which protects DELOS-SUSP methodology, owned by Nanomol Technologies SL, and stock ownership in Nanomol Technologies SL.

Data Availability Statement

The data that supports the findings of this study are available in the supplementary material of this article. Additional data is available on request from the corresponding authors.

Keywords

cancer therapy, miRNAs delivery, nanocarriers, nanovesicles, neuroblastoma, pediatric cancer, quatsomes, siRNAs delivery

Received: September 2, 2021
Revised: October 15, 2021
Published online: November 16, 2021

[1] K. D. Warner, C. E. Hajdin, K. M. Weeks, *Nat. Rev. Drug Discovery* **2018**, *17*, 547.
[2] A. Soriano, L. Jubierre, A. Almazan-Moga, C. Molist, J. Roma, J. S. de Toledo, S. Gallego, M. F. Segura, *Pharmacol. Res.* **2013**, *75*, 3.

[3] S. W. L. Lee, C. Paoletti, M. Campisi, T. Osaki, G. Adriani, R. D. Kamm, C. Mattu, V. Chiono, *J. Controlled Release* **2019**, *313*, 80.
[4] J. Shi, P. W. Kantoff, R. Wooster, O. C. Farokhzad, *Nat. Rev. Cancer* **2017**, *17*, 20.
[5] B. Ozpolat, A. K. Sood, G. Lopez-Berestein, *J. Intern. Med.* **2010**, *267*, 44.
[6] I. Fernandez-Pineiro, I. Badiola, A. Sanchez, *Biotechnol. Adv.* **2017**, *35*, 350.
[7] D. Haussecker, *J. Controlled Release* **2014**, *195*, 49.
[8] C. L. Daige, J. F. Wiggins, L. Priddy, T. Nelligan-Davis, J. Zhao, D. Brown, *Mol. Cancer Ther.* **2014**, *13*, 2352.
[9] R. Kanasty, J. R. Dorkin, A. Vegas, D. Anderson, *Nat. Mater.* **2013**, *12*, 967.
[10] N. Grimaldi, F. Andrade, N. Segovia, L. Ferrer-Tasies, S. Sala, J. Veciana, N. Ventosa, *Chem. Soc. Rev.* **2016**, *45*, 6520.
[11] G. Bozzuto, A. Molinari, *Int. J. Nanomed.* **2015**, *10*, 975.
[12] Y. P. Patil, S. Jadhav, *Chem. Phys. Lipids* **2014**, *177*, 8.
[13] E. Miele, G. P. Spinelli, E. Miele, E. Di Fabrizio, E. Ferretti, S. Tomao, A. Gulino, *Int. J. Nanomed.* **2012**, *7*, 3637.
[14] H. Y. Xue, S. Liu, H. L. Wong, *Nanomedicine* **2014**, *9*, 295.
[15] A. Bouchie, *Nat. Biotechnol.* **2013**, *31*, 577.
[16] N. van Zandwijk, N. Pavlakis, S. C. Kao, A. Linton, M. J. Boyer, S. Clarke, Y. Huynh, A. Chrzanowska, M. J. Fulham, D. L. Bailey, W. A. Cooper, L. Kritharides, L. Ridley, S. T. Pattison, J. MacDiarmid, H. Brahmbhatt, G. Reid, *Lancet Oncol.* **2017**, *18*, 1386.
[17] L. F. Gebert, M. A. Rebhan, S. E. Crivelli, R. Denzler, M. Stoffel, J. Hall, *Nucleic Acids Res.* **2014**, *42*, 609.
[18] L. Ferrer-Tasies, E. Moreno-Calvo, M. Cano-Sarabia, M. Aguilella-Arzo, A. Angelova, S. Lesieur, S. Ricart, J. Faraudo, N. Ventosa, J. Veciana, *Langmuir* **2013**, *29*, 6519.
[19] E. Elizondo, J. Larsen, N. S. Hatzakis, I. Cabrera, T. Bjornholm, J. Veciana, D. Stamou, N. Ventosa, *J. Am. Chem. Soc.* **2012**, *134*, 1918.
[20] I. Cabrera, E. Elizondo, O. Esteban, J. L. Corchero, M. Melgarejo, D. Pulido, A. Cordoba, E. Moreno, U. Unzueta, E. Vazquez, I. Abasolo, S. SchwartzJr., A. Villaverde, F. Albericio, M. Royo, M. F. Garcia-Parajo, N. Ventosa, J. Veciana, *Nano Lett.* **2013**, *13*, 3766.
[21] G. Vargas-Nadal, M. Munoz-Ubeda, P. Alamo, M. Mitjans, V. Cespedes, M. Kober, E. Gonzalez-Mira, L. Ferrer-Tasies, M. P. Vinardell, R. Mangues, J. Veciana, N. Ventosa, *Nanomedicine* **2020**, *24*, 102136.
[22] X. Liu, A. Ardizzone, B. Sui, M. Anzola, N. Ventosa, T. Liu, J. Veciana, K. D. Belfield, *ACS Omega* **2017**, *2*, 4112.
[23] A. Ardizzone, S. Kurhuzenkau, S. Illa-Tuset, J. Faraudo, M. Bondar, D. Hagan, E. W. Van Stryland, A. Painelli, C. Sissa, N. Feiner, L. Albertazzi, J. Veciana, N. Ventosa, *Small* **2018**, *14*, 1703851.
[24] J. Morla-Folch, G. Vargas-Nadal, T. Zhao, C. Sissa, A. Ardizzone, S. Kurhuzenkau, M. Kober, M. Uddin, A. Painelli, J. Veciana, K. D. Belfield, N. Ventosa, *ACS Appl. Mater. Interfaces* **2020**, *12*, 20253.
[25] M. S. Irwin, J. R. Park, *Pediatr. Clin. North Am.* **2015**, *62*, 225.
[26] K. K. Matthay, J. M. Maris, G. Schleiermacher, A. Nakagawara, C. L. Mackall, L. Diller, W. A. Weiss, *Nat. Rev. Dis. Primers* **2016**, *2*, 16078.
[27] A. Boloix, L. Paris-Coderch, A. Soriano, J. Roma, S. Gallego, J. S. de Toledo, M. F. Segura, *Ann. Pediatr.* **2016**, *85*, 109.e1.
[28] A. Soriano, M. Masanas, A. Boloix, N. Masia, L. Paris-Coderch, O. Piskareva, C. Jimenez, K. O. Henrich, J. Roma, F. Westermann, R. L. Stallings, C. Sabado, J. S. de Toledo, A. Santamaria, S. Gallego, M. F. Segura, *Cell. Mol. Life Sci.* **2019**, *76*, 2231.
[29] H. Takahashi, K. Sinoda, I. Hatta, *Biochim. Biophys. Acta* **1996**, *1289*, 209.
[30] L. Hosta-Rigau, Y. Zhang, B. M. Teo, A. Postma, B. Stadler, *Nanoscale* **2013**, *5*, 89.
[31] P. C. Barreleiro, R. P. May, B. Lindman, *Faraday Discuss.* **2003**, *122*, 191.
[32] N. Dan, D. Danino, *Adv. Colloid Interface Sci.* **2014**, *205*, 230.
[33] S. Huebner, B. J. Battersby, R. Grimm, G. Cevc, *Biophys. J.* **1999**, *76*, 3158.
[34] L. Desigaux, M. Sainlos, O. Lambert, R. Chevre, E. Letrou-Bonneval, J. P. Vigneron, P. Lehn, J. M. Lehn, B. Pitard, *Proc. Natl. Acad. Sci. U. S. A.* **2007**, *104*, 16534.
[35] M. Gujrati, A. Malamas, T. Shin, E. Jin, Y. Sun, Z. R. Lu, *Mol. Pharmaceutics* **2014**, *11*, 2734.
[36] P. Resnier, T. Montier, V. Mathieu, J. P. Benoit, C. Passirani, *Biomaterials* **2013**, *34*, 6429.
[37] A. Wittrup, A. Ai, X. Liu, P. Hamar, R. Trifonova, K. Charisse, M. Manoharan, T. Kirchhausen, J. Lieberman, *Nat. Biotechnol.* **2015**, *33*, 870.
[38] A. Soriano, L. Paris-Coderch, L. Jubierre, A. Martinez, X. Zhou, O. Piskareva, I. Bray, I. Vidal, A. Almazan-Moga, C. Molist, J. Roma, J. R. Bayascas, O. Casanovas, R. L. Stallings, J. S. de Toledo, S. Gallego, M. F. Segura, *Oncotarget* **2016**, *7*, 9271.
[39] M. Ha, V. N. Kim, *Nat. Rev. Mol. Cell Biol.* **2014**, *15*, 509.
[40] E. Persi, M. Duran-Frigola, M. Damaghi, W. R. Roush, P. Aloy, J. L. Cleveland, R. J. Gillies, E. Ruppin, *Nat. Commun.* **2018**, *9*, 2997.
[41] K. A. White, B. K. Grillo-Hill, D. L. Barber, *J. Cell Sci.* **2017**, *130*, 663.
[42] P. Swietach, *Cancer Metastasis Rev.* **2019**, *38*, 5.
[43] B. A. Webb, M. Chimenti, M. P. Jacobson, D. L. Barber, *Nat. Rev. Cancer* **2011**, *11*, 671.
[44] R. A. Cardone, K. O. Alfarouk, R. L. Elliott, S. S. Alqahtani, S. B. M. Ahmed, A. N. Aljarbou, M. R. Greco, S. Cannone, S. J. Reshkin, *Int. J. Mol. Sci.* **2019**, *20*, 3694.
[45] J. Lukas, H. Muller, J. Bartkova, D. Spitkovsky, A. A. Kjerulff, P. Jansen-Durr, M. Strauss, J. Bartek, *J. Cell Biol.* **1994**, *125*, 625.
[46] P. Hydbring, A. Castell, L. G. Larsson, *Genes* **2017**, *8*, 174.
[47] P. Pandi, A. Jain, N. Kommineni, M. Ionov, M. Bryszewska, W. Khan, *Int. J. Pharm.* **2018**, *550*, 240.
[48] L. Zhang, X. Yang, Y. Lv, X. Xin, C. Qin, X. Han, L. Yang, W. He, L. Yin, *Sci. Rep.* **2017**, *7*, 46186.
[49] B. Shi, E. Keough, A. Matter, K. Leander, S. Young, E. Carlini, A. B. Sachs, W. Tao, M. Abrams, B. Howell, L. Sepp-Lorenzino, *J. Histochem. Cytochem.* **2011**, *59*, 727.
[50] D. L. Jasinski, H. Li, P. Guo, *Mol. Ther.* **2018**, *26*, 784.
[51] V. Fehring, U. Schaeper, K. Ahrens, A. Santel, O. Keil, M. Eisermann, K. Giese, J. Kaufmann, *Mol. Ther.* **2014**, *22*, 811.
[52] J. Park, Y. Pei, J. Xu, Y. Yeo, *Adv. Drug Delivery Rev.* **2016**, *104*, 93.
[53] S. Kawakami, A. Sato, M. Nishikawa, F. Yamashita, M. Hashida, *Gene Ther.* **2000**, *7*, 292.
[54] J. Merlo-Mas, J. Tomsen-Melero, J. L. Corchero, E. Gonzalez-Mira, A. Font, J. N. Pedersen, N. Garcia-Aranda, E. Cristobal-Lecina, M. Alcaina-Hernando, R. Mendoza, E. Garcia-Fruitos, T. Lizarraga, S. Resch, C. Schimpel, A. Falk, D. Pulido, M. Royo, S. SchwartzJr., I. Abasolo, J. S. Pedersen, D. Danino, A. Soldevila, J. Veciana, S. Sala, N. Ventosa, A. Cordoba, *J. Supercrit. Fluids* **2021**, *173*, 105204.
[55] K. J. Livak, T. D. Schmittgen, *Methods* **2001**, *25*, 402.
[56] C. A. Schneider, W. S. Rasband, K. W. Eliceiri, *Nat. Methods* **2012**, *9*, 671.